The effects of oxygen plasma and humidity on surface roughness, water contact angle and hardness of silicon, silicon dioxide and glass

IOP Publishing Journal of Micromechanics and Microengineering
J. Micromech. Microeng. **24** (2014) 035010 (14pp) doi:10.1088/0960-1317/24/3/035010

The effects of oxygen plasma and humidity on surface roughness, water contact angle and hardness of silicon, silicon dioxide and glass

A U Alam, M M R Howlader and M J Deen

Department of Electrical and Computer Engineering, McMaster University, 1280 Main Street West, Hamilton, Ontario, L8S 4K1, Canada

E-mail: mrhowlader@ece.mcmaster.ca and jamal@mcmaster.ca

Received 10 September 2013, revised 18 December 2013
Accepted for publication 8 January 2014
Published 14 February 2014

Abstract

For heterogeneous integration in many More-than-Moore applications, surface preparation is the key step to realizing well-bonded multiple substrates for electronics, photonics, fluidics and/or mechanical components without a degradation in performance. Therefore, it is critical to understand how various processing and environmental conditions affect their surface properties. In this paper, we investigate the effects of oxygen plasma and humidity on some key surface properties such as the water contact angle, roughness and hardness of three materials: silicon (Si), silicon dioxide (SiO_2) and glass, and their impact on bondability. The low surface roughness, high surface reactivity and high hydrophilicity of Si, SiO_2 and glass at lower activation times can result in better bondability. Although, the surface reactivity of plasma-ambient-humidity-treated Si and SiO_2 is considerably reduced, their reduction of roughness and increase of hydrophilicity may enable good bonding at low temperature heating due to augmented hydroxyl groups. The decrease of hardness of Si and SiO_2 with increased activation time is attributed to higher surface roughness and the formation of amorphous layers of Si. While contact angle and surface roughness results show a correlation with bondability, the role of hardness on bondability requires further investigation.

Keywords: surface roughness, water contact angle, hardness, oxygen plasma bonding, humidity

(Some figures may appear in colour only in the online journal)

1. Introduction

A major challenge in the semiconductor industry is heterogeneous integration of multiple technologies for emerging health, environmental, transportation or security applications. In heterogeneous integration, it is critical that the surfaces of the various substrates to be integrated onto a common platform be properly cleaned and activated. In fact, the surface of the substrates is one of the most important factors controlling the physical, chemical, electro-optical and microfluidic properties of new lab-on-chip, sensing or medical diagnostic systems. For these new systems in the More-than-Moore ITRS (International Technology Roadmap of Semiconductors) [1] scenario, diverse materials including silicon (Si) [2], silicon dioxide (SiO_2) [3] and Pyrex glass [4] are commonly used for the assembly of integrated heterogeneous systems. For example, the heterogeneous integration of silicon-based electronics with photonics components [5, 6], MEMS components such as electrokinetic pumps or cell processing modules, polymer-based filtration systems [7, 8], and silicon- or polymer-based sensors with microfabricated reference electrodes [7, 9, 10], all require the bonding of one substrate to another. Examples of commonly-used substrates include silicon, silicon dioxide

or glass, on which the electronics, photonics, MEMS or fluidic components or modules are fabricated and subsequently integrated to create lab-on-chip sensing [7] or imaging [11] systems. For these MEMS-based applications, an important requirement of the bonding or integration technique is that the performance and reliability of the individual modules should not be compromised after bonding [12]. To maintain performance and reliability, appropriate surface preparation before bonding is a key requirement.

Previously, various surface treatment techniques [13–18] have been utilized for their integration. One of the promising techniques is surface-activated bonding using oxygen reactive ion etching (O_2RIE) plasma [18]. The O_2RIE plasma modifies the hydrophilicity (i.e., contact angle), morphology (i.e., surface roughness) and mechanical properties (e.g., surface hardness) of the surfaces that affect the solid–solid interfaces in, for example, wafer bonding [19], and the solid–liquid interfaces in miniaturized biomedical systems [20, 21].

Contact angle measurement is critical to identifying the hydrophilicity of the surfaces in systems' integration. For example, in Si-based wafer bonding, an environment with high relative humidity containing OH groups resulted in a lower contact angle or higher hydrophilicity [22]. Near-surface nanohardness and contact angle measurements in plasma immersion ion implanted silicon wafers showed increased reliability for high-temperature microelectronics [23]. The surface charge and contact angle (i.e., surface reactivity) of SiO_2 films with argon (Ar) and H_2O plasma treatments and their aging behavior were investigated [24]. The H_2O plasma-treated surfaces showed higher compositional stability than that with Ar plasma treatment. Surface treatment using plasma polymerization was used for the fabrication of organic microfluidic devices on silicon/glass substrate [17]. The fluid velocity was increased up to 450 μm s^{-1} due to surface modification with plasma polymerized acrylic acid. A constant surface reactivity of Si and glass in microfluidic devices was achieved due to dichlorodimethylsilane chemical treatment [25]. Also, passive microfluidic valves were made using SiO_2/glass hydrophobic (contact angle $\sim$102°) micro-channels modified by self-assembled monolayer of octadecyltrichlorosilane and plasma deposited CHF_3 patterns [26].

The contact angle provides information about the chemical affinity of bonding surfaces. Surface roughness and surface mechanical properties such as material elasticity determine the contact quality of the integrated systems. For example, surface roughness was considered in the calculation of adhesion for the real area of contact in the direct wafer bonding [27]. In the laser bonding of Pyrex/Si, the bonding strength decreased almost linearly with the increase of surface roughness [28]. A direct correlation of surface roughness with bonding strength was also found by the bearing ratio (i.e., the ratio of the area above a given height to the total area) analysis of surface roughness. A decrease of effective bond strength with decreasing bearing ratio was reported [28]. In another study, surface roughness was decreased with increased temperature during hydrazine (a chemical propellant for satellites) treatment of Si/SiO_2/Si_3N_4 passivation layer for a hydrazine-based microthruster [29]. Also, surface topography related to the fatigue of poly-Si under the application of a wide range of cyclic voltages was studied. Nucleation and propagation of micro-cracks were observed. In fact, a surface smoothening effect was observed above a critical cyclic voltage of $\sim$140 V [30]. In the study of the nanomechanical properties of standard and strained SOI, thin bonded Si films showed a considerably lower hardness and modulus of elasticity than those of bulk single crystal Si [31]. Plasma activation techniques using NH_3, O_2 and H_2 were used to tune the hardness of SiO_2 thin films [32].

Recently, we have demonstrated the surface-activated bonding of Si/Ge, SiO_2/Ge and glass/glass using O_2RIE. The high hydrophilicity of the Si, Ge and SiO_2 surfaces were combined with their higher surface reactivity and low surface roughness to attain good bonding [33, 34]. But these results do not provide plasma activation time dependent surface hydrophilicity, morphology and hardness. The humidity induced hydrophilicity of silicon oxide resulting in degraded adhesion was reported [35]. Unfortunately, the role of the ambient and humidity storage on the surfaces has not yet been investigated. Moreover, there is a need to characterize the surfaces that are to be processed in a single research facility in order to avoid artifacts induced by the processing equipment. Thus a comprehensive investigation of O_2RIE plasma processed Si, SiO_2 and glass through water contact angle, surface roughness and hardness are needed.

This article investigates the influence of O_2RIE plasma and humidity on the water contact angle, roughness and hardness of Si, SiO_2 and glass surfaces affecting their bondability. To clarify the individual role of the plasma and humidity, the plasma activated surfaces were treated in different sequences in a clean room ambient, and/or in a humidity-reliability chamber at 15 °C and 98% RH. The water contact angle, roughness and hardness of the O_2RIE plasma-treated surfaces at different storage conditions were analyzed using a drop shape analyzer, an atomic force microscope (AFM) and an ultra-micro hardness tester.

2. Materials and methods

2.1. Preparation of materials

Three types of materials were used for the surface analysis: (i) one-side mirror polished p-type Si(1 0 0) wafers of 450 μm thickness; (ii) SiO_2-on-Si wafers with 50 nm thick thermal oxides; and (iii) glass (from SCHOTT, US) wafers. The as-received Si wafers have native oxides of thickness $\sim$2 nm [13]. The wafers were cut into 10 $\times$ 10 mm^2 pieces using diamond needle. The O_2RIE plasma activations were performed for three sets of Si and SiO_2 pieces. In each set, there were three pieces of wafers for each activation time, which were used for roughness, hardness and contact angle measurement, respectively. The plasma activation time ranged from 60 to 1200 s. Although typical wafer bonding techniques [36] do not use such a high activation time for surface treatment, we utilized this large range in order to clearly identify the effect of plasma activation on other bonding parameters

Table 1. Description of the materials, their surface activation and storage conditions with their corresponding acronyms.

Acronyms	Surface activation	Storage conditions	Materials
Si:O_2RIE	O_2RIE plasma	No storage	Si
Si:O_2RIE+20RH	O_2RIE plasma	20 days of storage in 98% RH and 15 °C temperature	Si
Si:O_2RIE:20D+20RH	O_2RIE plasma	20 days of storage in class 1000 cleanroom ambient and 20 days in 98% RH and 15 °C temperature	Si
SiO_2:O_2RIE	O_2RIE plasma	No storage	SiO_2
SiO_2:O_2RIE+20RH	O_2RIE plasma	20 days of storage in 98% RH and 15 °C temperature	SiO_2
SiO_2:O_2RIE+20D+20RH	O_2RIE plasma	20 days of storage in class 1000 cleanroom ambient and 20 days in 98% RH and 15 °C temperature	SiO_2
Glass:O_2RIE	O_2RIE plasma	No storage	Glass

(i.e., hydrophilicity, roughness and hardness). Table 1 shows the three sets of Si and SiO_2 specimens and one set of glass specimens along with their activation time, storage conditions and acronyms. The first set of wafers was analyzed right after the O_2RIE plasma activation. The second set was analyzed after storing in 98% relative humidity for 20 days. The third set was analyzed after storing in clean room ambient (class 1000, 23 °C and 45% RH) for 20 days as well as for 20 days in 15 °C temperature and 98% relative humidity to investigate their storage behavior. In the case of glass, there was only one set of wafers. It was analyzed right after the plasma activation. These humidity and ambient conditions were chosen to identify the aging processes [37] in the surfaces that control the bonding and packaging of MEMS. The temperature of the humidity chamber was held at 15 °C to achieve the highest humidity. In order to denote different sets of wafers with different activation times and storage conditions, we will use the acronyms defined in the following.

2.2. Oxygen plasma activation

The wafer surfaces were activated in a low vacuum pressure using a 13.85 MHz oxygen O_2RIE plasma in a hybrid plasma bonder (HPB) from the Bondtech^{TM} Corporation. More details about the oxygen RIE plasma generation are provided elsewhere [18]. The different plasma activation times selected were 60 s, 150 s, 300 s, 600 s and 1200 s. The plasma power was 300 W and the pressure during plasma glow was 200 Pa.

2.3. Atomic force microscopy (AFM)

The surface roughness was measured using a dimension icon AFM from the Bruker Corporation. A Si RTSPA tip was used in standard tapping mode with a scan area of 2 × 2 μm^2. The surface roughness (R_q) was measured using the root mean square (RMS) method. Other roughness parameters such as maximum height (R_z), skewness (S_{ku}) and kurtosis (R_{ku}) were also measured.

2.4. Contact angle measurement

The water contact angle was measured using a drop shape analysis system (DSA100) from KRÜSS with a 6 μl de-ionized water droplet. The contact angle measurement of the first set of wafers after O_2RIE activation was delayed for approximately 3 min due to the transfer of specimens from the HPB to the DSA100 workstation. The sessile drop method [38] was used for the contact angle measurements. The contact angles of each specimen were measured once every second for 2 min of elapsed time to get an average contact angle.

2.5. Martens' hardness measurement

The Martens' hardness of surfaces was measured using a SHIMADZU Dynamic Ultra-micro Hardness Tester (DUH-211S). A triangular pyramid indenter with a tip angle of 115° was used. The Martens' hardness is calculated from the applied test force versus indentation depth curve when increasing the test force, using the following formula [39]:

$$HM = \frac{1000F}{26.43 \times h^2}[\text{Unit: N/mm}^{-2}],$$

where F = applied test force (mN) and h = indentation depth (μm). Two types of tests were conducted for the hardness measurement, load–unload test and cycle test. In the load–unload test mode, the indenter force is increased to a preset maximum force, held at this force for a specified time and then the indenter is unloaded. The cycle test indentation experiment consists of several steps, such as approaching the surface; loading to maximum force; holding the force for a specified time; unloading to minimum force; reloading to peak force again; holding the force again; and so on. The preset maximum test force for both the load–unload test and the cycle test was 10 mN. In the cycle test, the number of cycles was five. The reason for using a very low test force was to measure the nanoindentation hardness, which is related to only the treated surface and where the size of the residual impression is often only a few microns [40].

2.6. Humidity and reliability chamber

Specimens were stored in a humidity-reliability chamber from ESPEC. The temperature and relative humidity was held constant at 15 °C and 98% RH. The temperature and humidity range of the chamber was −35 to 180 °C and 10% to 98% RH. The temperature accuracy was ±0.3 °C, and that of the humidity was ±2.5% RH.

3. Results and discussions

3.1. Surface roughness

Figures 1 and 2 show the typical three-dimensional (3D) AFM images of Si and SiO_2 wafer surfaces before and after

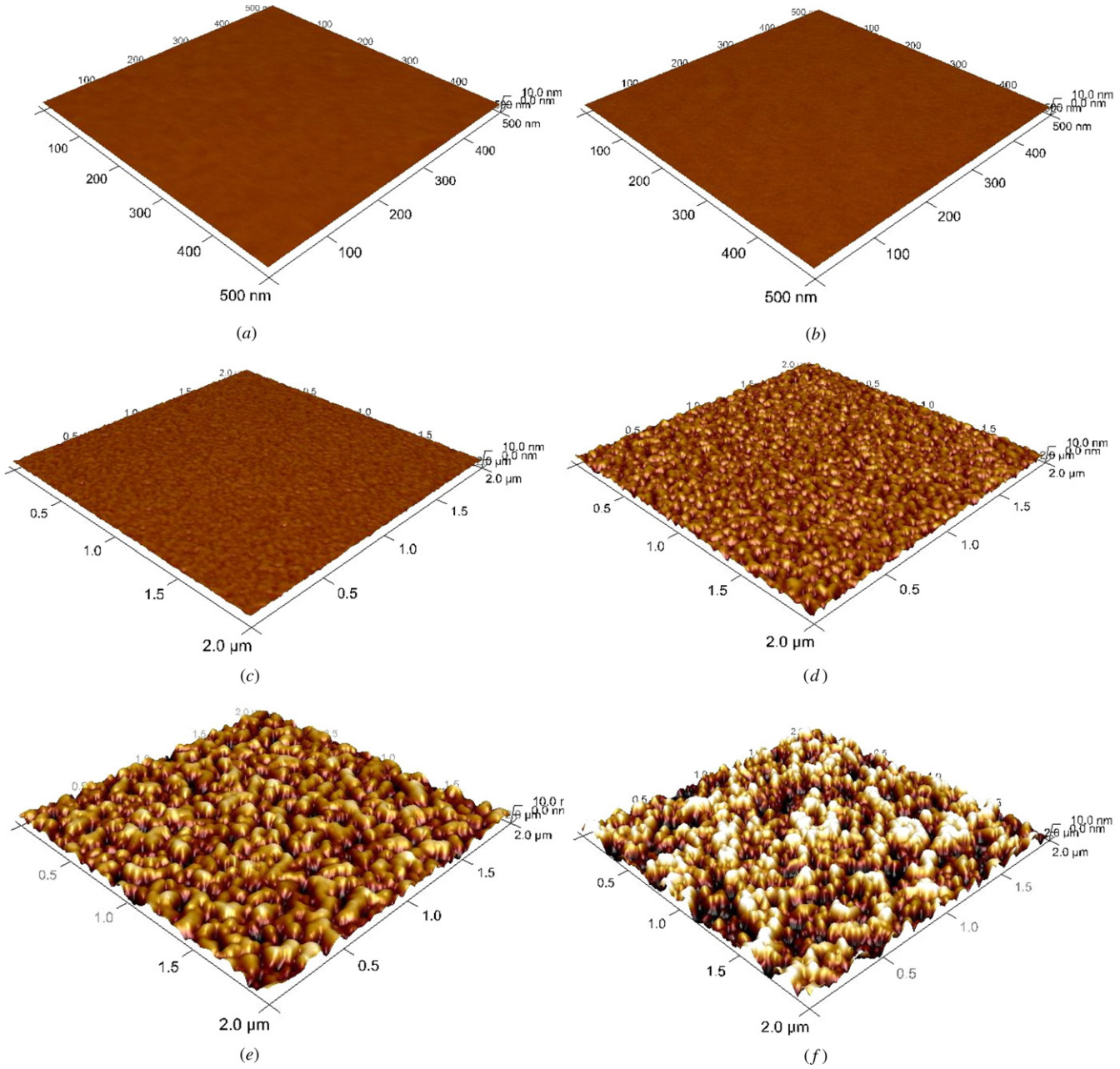

Figure 1. Three-dimensional (3D) atomic force microscope (AFM) images of Si wafer surfaces before and after O_2RIE plasma activation time. The RMS surface roughness (R_q) due to the corresponding plasma treatment times are given in the image titles. (*a*) As-received Si ($R_q = 0.12$ nm), (*b*) O_2RIE 60 s ($R_q = 0.16$ nm), (*c*) O_2RIE 150 s ($R_q = 0.43$ nm), (*d*) O_2RIE 300 s ($R_q = 1.23$ nm), (*e*) O_2RIE 600 s ($R_q = 3.70$ nm), (*f*) O_2RIE 1200 s ($R_q = 5.78$ nm).

O_2RIE plasma activation for different times. Figure 3 shows the RMS surface roughness of Si, SiO_2 and glass at different surface activation times and storage conditions. Table 2 summarizes the surface roughness parameters of Si, SiO_2 and glass specimens including RMS roughness, maximum height, skewness and kurtosis. The surface roughness of Si:O_2RIE, increased with the increase of activation time. While the rate of increase of surface roughness was not significant until 300 s (figure 3(*a*)), it was considerable after 300 s. At lower activation times, the RIE plasma removed the native oxides, and it started etching as well as oxidizing at higher activation times. However, the rate of etching was higher than that of oxidation at the higher activation times. Thus, the highest surface roughness (∼6 nm) was measured at 1200 s. This is larger than in our previous study (∼1.68 nm) [41], where a lower plasma power and gas pressure were used [42, 43]. An increase of the surface roughness with increasing activation time for the Si:O_2RIE+20RH and Si:O_2RIE+20D+20RH specimens was also observed. However, they showed (figure 3(*a*)) reduced surface roughness as compared to Si:O_2RIE. This surface smoothening indicates the influence of high relative humidity on the Si surface. Surface smoothening was also reported [43] for Ge after oxygen plasma activation and rinsing with DI water due to

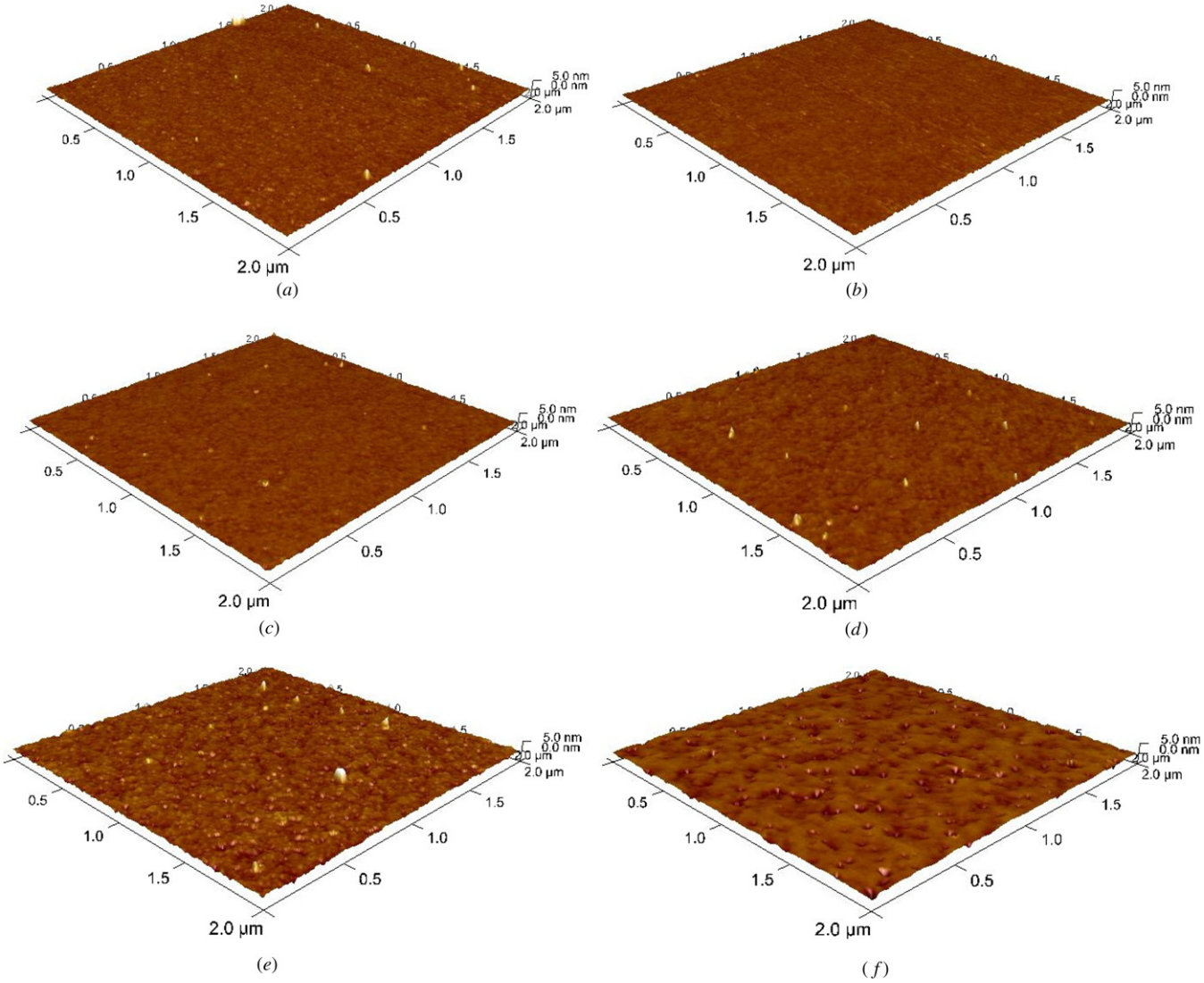

Figure 2. Three-dimensional (3D) atomic force microscope (AFM) images of SiO_2 wafer surfaces before and after O_2RIE plasma activation time. The RMS surface roughness (R_q) due to the corresponding plasma treatment times are given in the image titles. (*a*) As-received SiO_2 ($R_q = 0.22$), (*b*) O_2RIE 60 s ($R_q = 0.16$), (*c*) O_2RIE 150 s ($R_q = 0.20$), (*d*) O_2RIE 300 s ($R_q = 0.26$), (*e*) O_2RIE 600 s ($R_q = 0.38$), (*f*) O_2RIE 1200 s ($R_q = 0.44$).

the removal of the soluble GeO_2 layer and other defects. The modified surface was mainly terminated by hydroxyl groups. Although in our study, the plasma activated Si surfaces were not rinsed with DI water, their storage in ambient and 98% relative humidity for a long period of time caused the accumulation of water molecules due to their strong affinity with the hydroxyl group [44]. Moreover, a high surface roughness at higher plasma activation times increased the total surface area [43], which resulted in higher chemical affinity with the OH groups.

The surface roughness of SiO_2:O_2RIE at 60 s (figure 3(*b*)) was lower than that of as-received SiO_2 (i.e., before activation). A similar surface roughness reduction of SiO_2 was also observed [45] where the surface was treated by an RIE plasma with 50 mT oxygen atmosphere and treatment time higher than 10 s. Such a smoothening effect was attributed to the surface cleaning of, for example, hydrocarbons. On the other hand, the lower surface roughness of as-received SiO_2 after humidity treatment was due to the accumulation of OH groups from the humidity chamber. In both the cases (i.e., SiO_2:O_2RIE and SiO_2:O_2RIE+20RH), the surface roughness increased with increased activation time and their amplitudes of roughness were identical. While the surface roughness of the as-received Si (0.2 nm) and SiO_2 (0.22 nm) were identical, their plasma treatment and humidity storage at identical conditions showed the higher roughness of Si than that of SiO_2. This difference is due to the higher etching rate of Si than SiO_2 during O_2RIE activation. This phenomena is also described in [13], where plasma activation before Si/Si bonding resulted in more surface damage than that of Si/SiO_2 bonding. Unlike Si and SiO_2, the surface roughness of glass increased significantly after 60 s of activation to about ten times (figure 3(*c*)). A further increase of the activation time until 600 s did not result in a significant change in the surface roughness. The

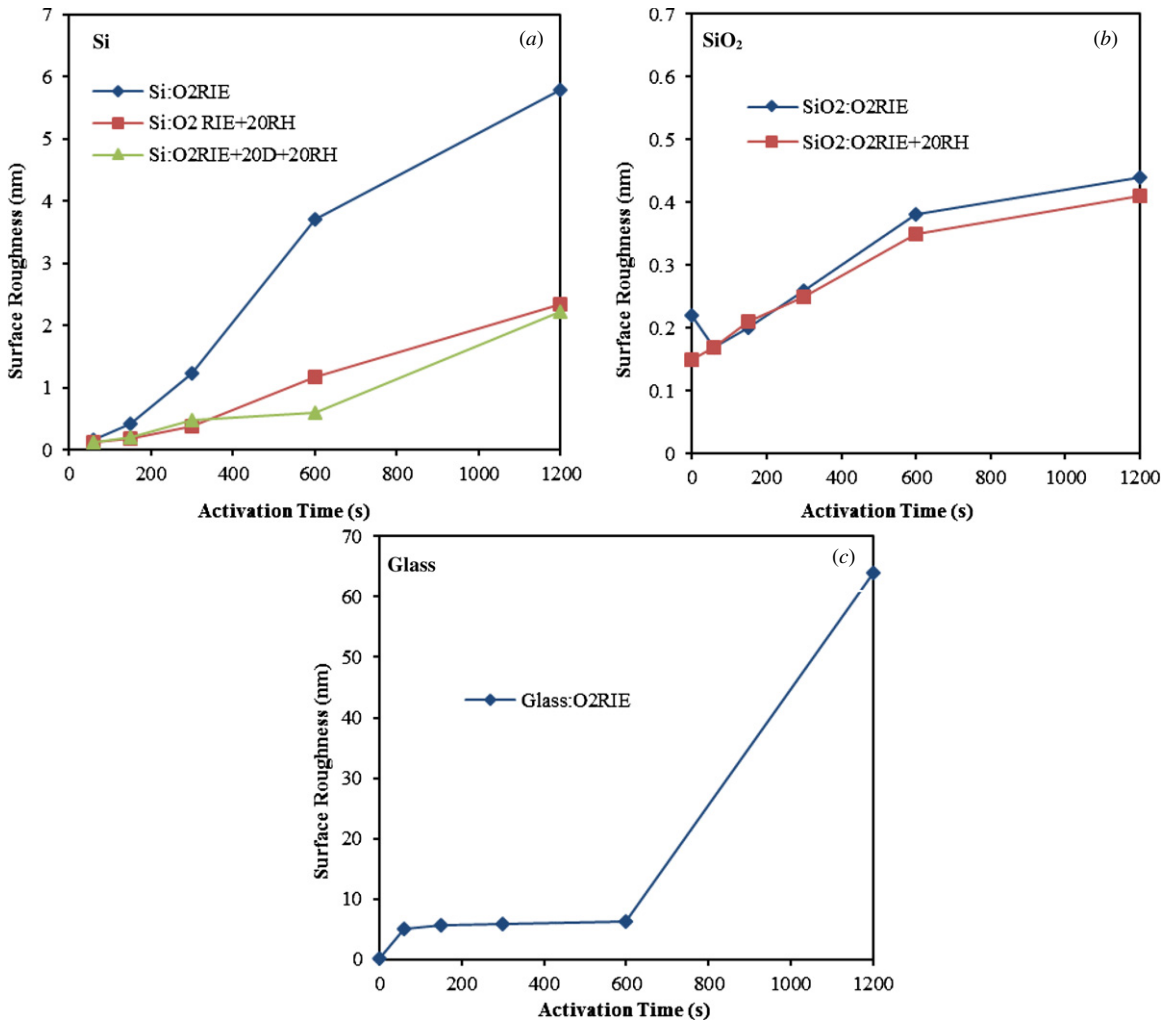

Figure 3. Surface roughness of (*a*) Si as a function of O_2RIE plasma activation time for different storage conditions, (*b*) SiO_2 as a function of O_2RIE plasma activation time for different storage conditions, and (*c*) glass as a function of O_2RIE plasma activation time. An activation time of 0 s means the as-received condition.

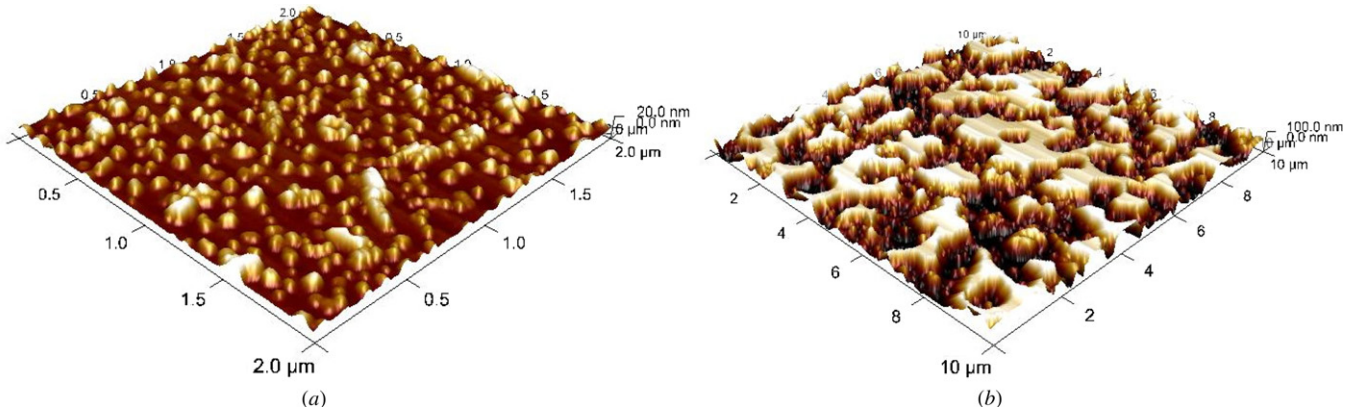

Figure 4. 3D AFM images of glass wafer surfaces at 300 s and 1200 s of O_2RIE plasma activation time. The RMS surface roughness (R_q) is given in the image titles. (*a*) O_2RIE 300 s ($R_q = 5.9$ nm), (*b*) O_2RIE 1200 s ($R_q = 63.9$ nm).

AFM images are identical for the surfaces activated from 60 to 600 s. An AFM image at 150 s is shown in figure 4(*a*). The activated glass surfaces had island-like nanostructures with varying heights of 5–7 nm. In fact, at 1200 s the glass was severely damaged causing a high surface roughness of about 63 nm (figure 4(*b*)).

The lower surface roughness of Si until 300 s (figure 3(*a*)) is suitable for hydrophilic bonding due to its added benefit

Table 2. Surface parameters of Si, SiO_2 and glass for different activation times and humidity and/or ambient storage conditions.

Specimen	Activation time (s)	RMS roughness, R_q (nm)	Maximum height, R_z (nm)	Skewness S_{ku}	Kurtosis R_{ku}
Si:O_2RIE	As-received (0)	0.12	0.988	0.174	3.05
	60	0.16	1.32	0.0345	2.73
	150	0.43	3.41	−0.293	2.87
	300	1.23	11.2	−0.237	2.96
	600	3.74	29.0	−0.305	2.8
	1200	5.78	42.3	−0.127	3.03
Si:O_2RIE+20RH	60	0.13	1.21	−0.0091	3.04
	150	0.19	1.65	−0.0749	2.98
	300	0.39	4.36	−0.216	3.28
	600	1.18	7.13	−0.492	3
	1200	2.34	18.7	0.118	3.06
Si:O_2RIE+20D+20RH	60	0.13	2.78	−0.0743	4.64
	150	0.21	3.49	−0.263	5.06
	300	0.48	3.82	0.146	2.95
	600	0.60	4.83	−0.382	2.65
	1200	2.23	16.0	−0.0104	2.88
SiO_2:O_2RIE	As-received (0)	0.22	3.04	0.104	3.48
	60	0.17	2.09	−0.329	4.11
	150	0.20	4.86	0.745	12.7
	300	0.26	7.09	1.88	37.4
	600	0.38	5.86	−0.515	4.32
	1200	0.44	6.49	−1.78	10.2
SiO_2:O_2RIE+20RH	60	0.15	1.80	0.024	3.16
	150	0.17	2.31	0.0562	3.54
	300	0.21	5.88	2.59	38.3
	600	0.25	5.47	−0.706	5.55
	1200	0.35	10.0	1.79	29.5
Glass:O_2RIE	As-received (0)	0.28	6.23	3.1	31
	60	5.16	40.7	2.11	7.38
	150	5.81	34.5	1.39	4.6
	300	5.92	42.2	1.62	5.48
	600	6.38	86.4	1.09	7.64
	1200	63.92	358	−0.0101	2.03

of higher hydrophilicity. Lower surface roughness allows an increased area of adhesion between contacting surfaces. This is because the surface roughness determines the contact area between the wafers in the bonding. Also, the bearing ratio analysis of the surface morphology of Si wafers revealed clear correlation of bonding strength with surface roughness (i.e., the bearing ratio) [46]. The bearing ratio is a quantity which describes how much surface area is lying above a given depth (i.e., the bearing depth). The higher the surface roughness, the lower the bearing ratio, which means less surface area for bonding. Therefore, surface roughness controls the adhesion between the bonding surfaces [27, 46], the interface void [47] and the hermetic sealing performance of MEMS and microfluidic devices [48], for example. On the other hand, the roughness of SiO_2 may not have a significant impact on the bonding due to its lower value (higher smoothness) than that of Si. In addition, the reduction of the surface roughness of Si to less than that of SiO_2 after humidity and ambient/humidity storage indicates that the Si surface accumulates more water molecules. Thus, SiO_2 is suitable for passivation for MEMS applications. Also, the high surface roughness of glass at prolonged activation may not be suitable for direct wafer bonding.

A comparative study of surface roughness parameters (table 2) shows that while the treated Si surfaces have a Gaussian height distribution ($S_{ku} = 0$, $R_{ku} = 3$), the treated SiO_2 and glass surfaces have non-Gaussian distributions (i.e., $S_{ku} \neq 0$) and $R_{ku} > 3$. These variations in S_{ku} and R_{ku} may have a potential impact on MEMS devices. According to the modeling of the effect of rough surfaces [49] on the static friction coefficient (μ), the high kurtosis and positive skewness of the O_2RIE plasma-treated SiO_2 and glass surfaces may result in a lower value of μ than that in the Gaussian distribution of the Si surface. This finding may be useful in MEMS devices when a low friction coefficient is desirable. Moreover, the 1200 s O_2RIE treated glass surface has unique surface topography (i.e., $R_{sk} = 0$ and $R_{ku} = 2.3$) as shown in figure 4(*b*). The lower kurtosis value and the lower Gaussian height distribution may result in a higher friction coefficient, which is not desirable in contact-mode micro-devices [50].

3.2. Water contact angle

To investigate the surface reactivity and hydrophilicity of Si, SiO_2 and glass in practical processing conditions for MEMS and microfluidics, we measured the contact angle of a DI water drop. Figure 5(*a*) shows the contact angle of a Si:O_2RIE surface for 2 min of elapsed time. As-received Si shows the highest contact angle, which remains almost constant

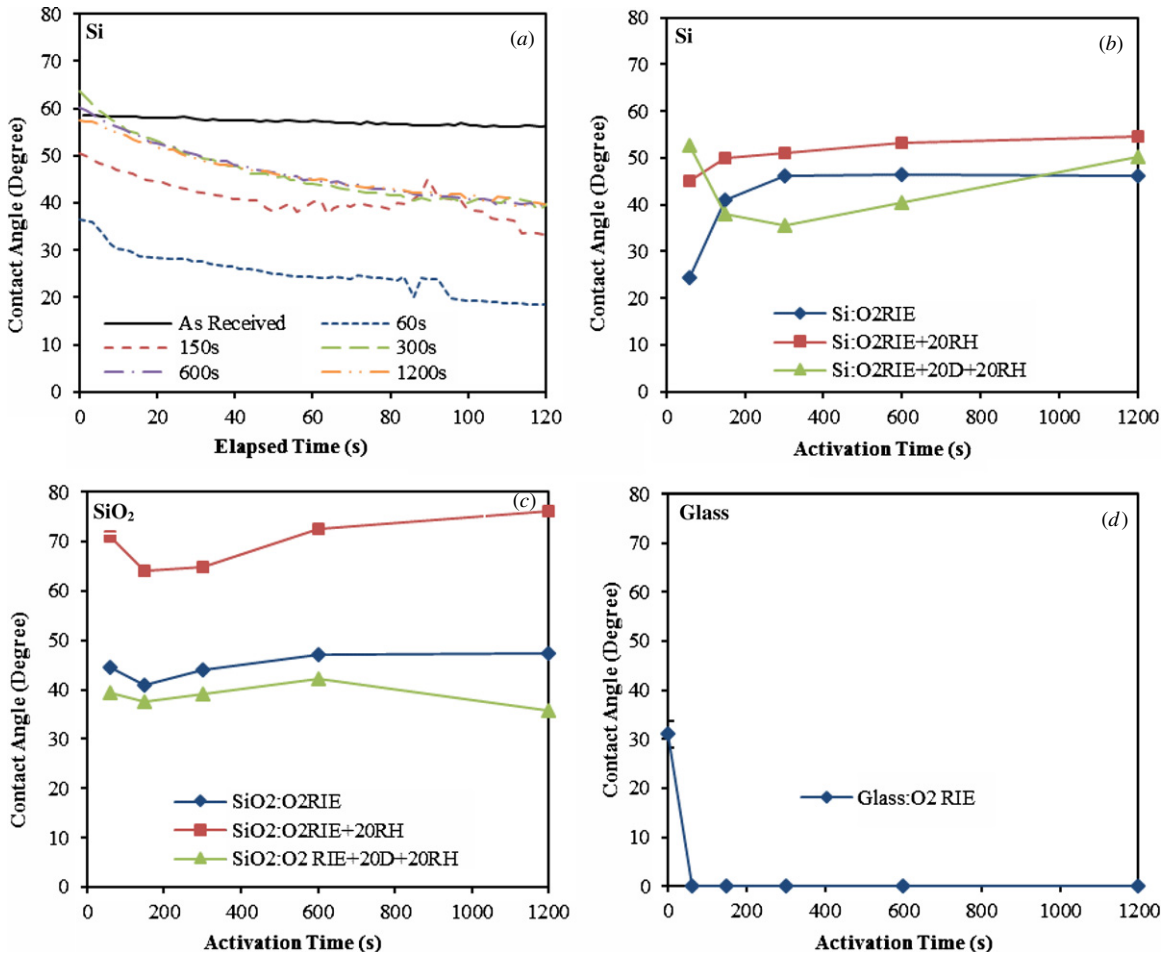

Figure 5. Contact angle of (*a*) Si as a function of elapsed time before and after O_2RIE plasma activation at different activation times for 60 to 1200 s; (*b*) Si as a function of O_2RIE plasma activation time for different storage conditions, (*c*) SiO_2 as a function of O_2RIE plasma activation time for different storage conditions, and (*d*) glass as a function of O_2RIE plasma activation time.

Table 3. Surface reactivity of Si, SiO_2 and glass at different activation times for different treatment and storage conditions.

	Surface reactivity (deg s^{-1})					
Specimen	As-received (0 s)	60 s	150 s	300 s	600 s	1200 s
Si:O_2RIE	0.02	0.12	0.09	0.16	0.15	0.14
Si:O_2RIE+20RH		0.02	0.03	0.02	0.03	0.04
Si:O_2RIE+20D+20RH		0.01	0.01	0.01	0.01	0.01
SiO_2:O_2RIE	0.02	0.08	0.11	0.10	0.12	0.12
SiO_2:O_2RIE+20RH	0.04	0.03	0.02	0.06	0.03	0.03
SiO_2:O_2RIE+20D+20RH	0.03	0.02	0.03	0.03	0.02	0.02
Glass:O_2RIE	0.05	–	–	–	–	–

throughout the elapsed time. The plasma activated Si shows a lower contact angle, and also the contact angle decreases with a higher rate. Thus, the contact angle information gives two kinds of surface properties: surface reactivity (i.e., the rate of decrease of contact angle throughout the measurement time), and surface hydrophilicity (i.e., the average contact angle). The contact angle is the measure of the surface energy that controls the quality of the hydrophilic wafer bonding. The lower contact angle results in higher hydrophilicity and a higher wetting of the surface [51]. The surface reactivity also governs the hydrophilicity since higher surface reactivity results in lower average contact angle (i.e. higher hydrophilicity). The summarized hydrophilicity of Si, SiO_2 and glass are shown in figures 5(*b*), (*c*) and (*d*), respectively. Each marker represents the average contact angle at that particular plasma activation time and storage condition. The surface reactivity (i.e., the rate of decrease of contact angle, unit deg s^{-1}) of Si, SiO_2 and glass is summarized in table 3. The surface reactivity and hydrophilicity control the bondability and reliability of MEMS and integrated heterogeneous systems [13].

The O_2RIE plasma activation removes the native surface oxide and creates a sub-surface oxide layer on Si wafers, as evident from the x-ray photoelectron spectroscopy results in [52]. The amount of $Si(-O)_2$ increases with the increase

in plasma activation time for Si:O_2RIE. The high surface reactivity of Si:O_2RIE (table 3) as compared to as-received Si is due to the removal of the native oxides and organic contaminants and the increased number of dangling bonds (free bonds) from broken Si-O and Si-H [51]. Similar surface reactivity behavior is also observed in the case of SiO_2:O_2RIE (table 3). The increased surface reactivity also leads to higher surface energy and hence increased adhesion and bonding strength in plasma bonded wafers [53]. The surface reactivity of SiO_2:O_2RIE is slightly lower than that of Si:O_2RIE, indicating the high bonding strength of Si-based wafer bonding [13, 54]. The glass: O_2RIE showed the highest surface reactivity, which makes it a promising candidate for anodic bonding [42]. The DI water drop quickly spread on the O_2RIE plasma-processed glass surface, which resulted in a contact angle that was below the measurement limit of the equipment. Storage in humidity (i.e., O_2RIE+20RH) and ambient/humidity (i.e., O_2RIE+20D+20RH) shows a significant reduction in the surface reactivity of Si and SiO_2 (table 3) due to the augmented -OH groups on the surface [41]. It has also been reported [43] that the surface reactivity of Si and SiO_2 are at a maximum immediately after the plasma activation, even though they remain hydrophilic in excess of 150 h after plasma activation. The highly reactive surface attracts particles from air when exposed in the ambient for a long period of time, which eventually decreases its surface reactivity as well as hydrophilicity.

The contact angles of as-received Si (figure 5(*a*)) and SiO_2 are almost identical (∼57°), and are higher than that of as-received glass (30°, figure 5(*d*)). Glass:O_2RIE shows the highest hydrophilicity (contact angle <5°) and Si:O_2RIE shows higher hydrophilicity (24.5°) than that of SiO_2:O_2RIE at 60 s. The contact angle values in this study vary slightly from other studies due to different plasma powers, activation times, chamber pressures and atmospheric exposure times. In a previous study, the contact angle of as-received SiO_2 was reported as 52° with a 9 μl DI water droplet, and the contact angle for O_2RIE plasma activated Si and SiO_2 was reported as 29.1° and 38.5°, respectively, with a flow rate of 50 sccm, a power of 200 W, a chamber pressure of 60 Pa and a plasma treatment time of 30 s [33]. In another study, the contact angle of oxygen plasma-treated glass was <5° at a plasma power of 140 W, a working pressure of 20 mTorr and a 60 s activation time [42].

With increasing activation time, the contact angle of Si increased until 300 s, and it became saturated at 600 s (46.5°) and 1200 s (46.2°). This is due to the increased surface roughness (see discussion in section 3.1) of Si:O_2RIE at higher activation times. Surface roughness obstructs the spreading of a water droplet in the contact angle measurements. A higher surface roughness creates a larger barrier to the spreading of water, a higher surface area in a smaller lateral space and more interaction with surrounding air, resulting in a larger contact angle and vice versa [36]. On the other hand, the contact angle of SiO_2:O_2RIE does not change significantly with activation time (figure 5(*c*)). The highly passivated SiO_2 layer is less likely to react with oxygen plasma. The highly hydrophilic surfaces form networks of hydrogen-bonded water molecules between the contacted wafers, which in turn creates Si-O-Si bonds resulting in enhanced bond strength [22]. Thus, the lower activation times of Si: O_2RIE can thus result in a good bonding strength due to the higher hydrophilicity and reactivity of the surface (figure 5(*b*)). On the other hand, higher contact angles in the case of Si:O_2RIE+20RH (figure 5(*b*)) and SiO_2:O_2RIE+20RH (figure 5(*c*)) reflect their reduced surface reactivity and less hydrophilicity due to the passivation of the dangling bonds.

The initial decrease of the contact angle of Si:O_2RIE+20D+20RH until 300 s and its increase afterwards (figure 5(*b*)) is attributed to the surface roughness induced variation in the amount of Si-$(OH)_x$ bonds [52]. Moreover, the decrease in contact angle for SiO_2:O_2RIE+20D+20RH (figure 5(*c*)) compared to that of SiO_2:O_2RIE was due to increased incorporation with OH groups from humidity and ambient. Thus Si and SiO_2 need proper passivation to reduce the risks of poor adhesion due to humidity-induced increased hydrophilicity in MEMS packaging [35]. Also, storage in ambient and humidity can result in good bondability (i.e., bonding strength), since the gap closing mechanism in room temperature direct wafer bonding requires water vapor from the ambient to initiate covalent bonding between the surfaces [55]. For further enhancement of bonding strength, a low temperature (i.e., 300 °C) heating for a short period of time (i.e., 2 h) was reported [41, 55]. The findings here can also be extended to the sequential plasma activated bonding (O_2RIE+nitrogen radicals) of Si/Si [51], Si/Pyrex glass [42], glass/glass [34], Si/Ge and SiO_2/Ge [33].

3.3. Surface hardness

Development of MEMS devices for the existing pressure sensing and force sensing systems [56], as well as for emerging applications such as energy harvesting [57], require materials that may go through different processing steps such as surface activation using plasma for the bonding, integration and packaging of MEMS devices [58]. Therefore, the nanoindentation hardness test is commonly used to evaluate the mechanical properties and reliability of MEMS structures [59]. Figure 6(*a*) shows a typical force–indentation depth curve applying a 10 mN peak force in the cycle test and load–unload test of as-received Si. The load–unload test has only one loading and unloading curve, whereas the cycle test has five. Both the cycle tests and load–unload tests were done in five and ten different positions, respectively, for each specimen. The indentation depths were slightly above 0.1 μm, which is the depth resolution in our system for the substrates investigated and the force used. Figures 5(*d*)–(*f*) and (*g*)–(*i*) show the summarized Martens' hardness results for Si and SiO_2, respectively, for different activation times and storage conditions. Hereafter, the term hardness will be used instead of Martens' hardness. Each marker on the plot shows the average hardness and the error bar shows the standard deviation of the hardness from the average.

The dependence of the surface hardness of Si may be attributed to the crystal structure, deposited layers, absorbents, morphology and reactivity of the surfaces. For example, the

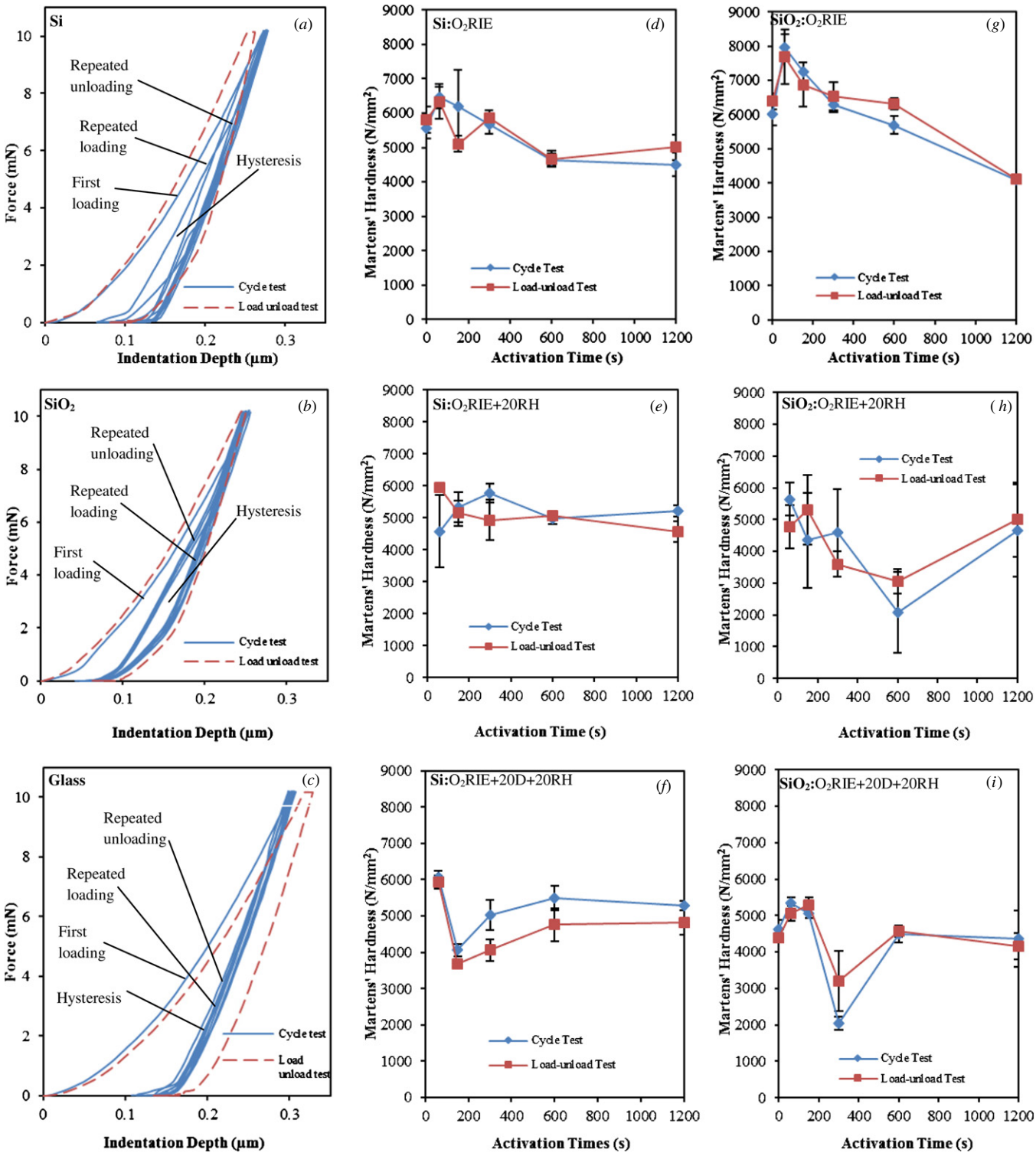

Figure 6. Indenter force versus indentation depth of (*a*) as-received Si, (*b*) as-received SiO_2, and (*c*) as-received glass, in the cycle test and the load–unload test for the analysis of Martens' hardness. Martens' hardness using the cycle test and the load–unload test as a function of O_2RIE plasma activation time for (*d*) Si without storing, (*e*) Si after storing in 98% relative humidity for 20 days, and (*f*) Si after storing in ambient for 20 days and in 98% relative humidity for 20 days, (*g*) SiO_2 without storing, (*h*) SiO_2 after storing in 98% relative humidity for 20 days, and (*i*) SiO_2 after storing in ambient for 20 days and in 98% relative humidity for 20 days.

loading–unloading process in the cycle test for as-received Si (figure 6(*a*)) shows hysteresis. It could be due to a pressure-induced phase transformation [49] of Si from diamond cubic form into β-tin form with a 22% decrease in volume. Since the surface roughness of the as-received Si and Si:O_2RIE at 60 s are identical, the lower hardness for the as-received Si (figure 6(*d*)) may be attributed to the native oxides and contaminants. Alternatively, the increase in hardness at 60 s is due to the removal of the native oxides. On the other hand, if only the lower deviation is considered at 150 s of Si:O_2RIE,

Table 4. Evolution of surface properties with the increase of oxygen plasma activation times at different storage conditions.

	Change in surface properties with the increase of activation times (60, 150, 300, and 600 s) under different storage conditions				
Surface treatment	Surface roughness	Surface reactivity	Hydrophilicity	Hardness	Bondability
Si:O_2RIE	Increases	High	High	Decreases	Better at lower activation time [41]
Si:O_2RIE+20RH	Slower increase than Si:O_2RIE	Low	Low	Slight decrease	Good at lower activation
Si:O_2RIE+20D+20RH	Similar to Si:O_2RIE+20RH	Very low	High	Overall decrease	Good at lower activation
SiO_2:O_2RIE	Slight increase	High	High	Decreases	Better at lower activation time
SiO_2:O_2RIE+20RH	Similar to SiO_2:O_2RIE	Low	Low	Slight decreases	Better at lower activation time
SiO_2:O_2RIE+20D+20RH	–	Very low	High	Overall decrease	Good at lower activation
Glass:O_2RIE	$\sim$ 5–10 nm	Very high	Very high	Negligible change	Better at low activation time

a decreasing trend in the hardness of Si is observed with the increase in activation time both in the cycle test and the load–unload test. This decrease could be related to higher surface roughness and changes in the atomic structure of the surfaces. The hardness of the plasma-induced oxide layers or the native oxide layers of Si wafers is below the measurement limit of the nanoindentation test equipment. The equipment can resolve a minimum depth of 0.1 μm (i.e., 100 nm), whereas the native oxide and sub-surface oxide layers are in the order of several nanometers. Thus the nanoindentation tests provide the hardness of surface/sub-surface oxide layers combined with the bulk material [60].

As discussed in the previous section, the surface roughness of Si increases with the increase of activation time. Therefore, higher surface roughness results in a lower contact area of the indenter tip, which causes an increase in the indentation depth observed in the depth versus force profiles. The indentation depth for the as-received Si and at low activation times (i.e., 60 s and 150 s) is lower ($\sim$0.26 μm) than that ($\sim$0.30 μm) of the higher activation times (i.e., 600 s and 1200 s). Therefore, the surface roughness controls the hardness of Si. It is also known that surface treatment using plasma having enough physical sputtering capability results in an amorphous layer [61]. The decrease of the hardness with increased activation time (figure 6(*d*)) may also be attributed to the formation of amorphous layer at higher plasma activation times. The formation of an amorphous layer in the plasma surface-activated wafer bonding was demonstrated elsewhere [62].

There was no considerable influence of humidity on the hardness of Si:O_2RIE+20RH (figure 6(*e*)). However, a decreasing trend in the hardness was observed in the load–unload test. Also, the rate of decrease of hardness for Si:O_2RIE+20RH with an increased activation time was lower than that of Si:O_2RIE in the load–unload test. Further storage in ambient/humidity (i.e., Si:O_2RIE+20D+20RH, figure 6(*f*)) caused a decrease in hardness ($\sim$6000 to $\sim$3500 N mm^{-2}) from 60 to 150 s and an eventual increase up to $\sim$5000 N mm^{-2} at 1200 s. The humidity, and the ambient/humidity storage induced variation in the hardness, is attributed to the quality of the complex formation of the absorbents (e.g., -OH) and deposited layers (e.g., carbon) on the surface. The surface reactivity determined by the relative composition of surface oxides due to hydroxyl groups (i.e., Si-OH) and sub-oxides (i.e., Si-O_2, Si-O_4) also may influence the hardness of Si.

The repeated force–indentation depth curves of the as-received SiO_2 (figure 6(*b*)) show higher hysteresis than that of Si (figure 6(*a*)). The hardness behavior of SiO_2:O_2RIE is identical to that of Si (figure 6(*g*)), except for its higher values from 60 to 600 s and its lower value at 1200 s. For SiO_2:O_2RIE+20RH (figure 6(*h*)), the hardness decreased except for 1200 s of activation time both in the load–unload test and the cycle test. On the other hand, for SiO_2:O_2RIE+20D+20RH (figure 6(*i*)), the hardness values in load–unload tests did not change significantly if only the upper deviation at 300 s was considered. Unlike Si, the surface roughness may not have a significant impact on the reduction of hardness, since SiO_2 shows a small increase in surface roughness with increased activation time. The role of deposited oxides, hydroxyl layers/absorbents and surface reactivity on the hardness of SiO_2 is not clear from this study due to its higher hardness than that of the surface additives. Unlike Si and SiO_2, glass showed the least hysteresis (figure 6(*c*)). Also, the change in the hardness ($\sim$4000 N mm^{-2}, not shown in figure 6) of glass:O_2RIE was insignificant with the increase in activation time except for at 1200 s, where it reduced to almost half ($\sim$2000 N mm^{-2}). This reduction in the hardness may be attributed to the severe damage of the glass surface after such a long activation time. The surface roughness of glass for this condition increased by more than ten times that of the as-received specimen.

A comparison among the O_2RIE treated specimens (figures 5(*d*), (*g*) and Glass:O_2RIE) shows that SiO_2 has the highest hardness and glass has the lowest hardness for identical conditions of activation time. The loading and unloading curves provide the plastic and elastic deformation of the surface [63]. Whereas, the as-received glass has an elasticity of $\sim 7.5 \times 10^4$ N mm^{-2}, the elasticity of the as-received Si and SiO_2 surfaces is almost equal, and is about $\sim 1.2 \times 10^5$ N mm^{-2}. Thus, the glass has a lower plastic deformation compared to Si and SiO_2. The lower plastic deformation of glass makes it a good candidate material for microfluidic devices with other polymer or flexible materials [64]. A comparison in the change of the surface properties of

the specimens with increase in activation time is summarized in table 4.

4. Conclusions

The water contact angle, roughness and hardness of oxygen reactive ion etching (O_2RIE) plasma activated silicon (Si), silicon dioxide (SiO_2) and glass surfaces with or without storage in ambient and 98% relative humidity were investigated. The summarized surface properties of Si, SiO_2 and glass are shown in table 4. The surface roughness for Si was increased with the increase of plasma activation time and it was higher than that of SiO_2. The surface roughness of the activated Si was reduced after treating it with humidity and air, but no change was observed in the SiO_2. This highly reduced roughness was due to higher accumulation of water molecules on Si surface. The surface roughness of glass suddenly increased after activation by an order of magnitude, then remained unchanged until 600 s and finally increased by another order of magnitude at 1200 s. This significantly increased roughness at 1200 s is due to surface damage. The low surface roughness at lower activation times is suitable for bonding.

The oxygen plasma activation of Si showed a lower contact angle and it showed an increasing trend with increasing activation time. Also, Si and SiO_2 showed high surface reactivity after plasma activation, which was considerably reduced after storage in humidity and ambient. The contact angle of the plasma-activated Si and SiO_2 surfaces was decreased due to the augmented -OH groups in ambient and humidity. Moreover, plasma-activated glass showed a highly reactive as well as hydrophilic surface that resulted in contact angles below 2°, which is beyond the detection limit. The high hydrophilicty and surface reactivity at lower activation times can result in better bondability. The high hydrophilicity after humidity–ambient treatment may also have good bondability provided that the surface contains OH groups.

The loading–unloading results in the hardness test identify hysteresis for Si, SiO_2 and glass due to the pressure-induced phase transformation. The hardness of Si and SiO_2 was decreased with increased activation time due to the higher surface roughness and the formation of amorphous layers (of Si). A considerable reduction in the hardness of the plasma-activated glass at 1200 s was observed due to the highly increased surface roughness. Furthermore, the humidity, and ambient/humidity storage induced variation was observed in Si and SiO_2. This dependence of the hardness is thought to be due to the quality of the complex formation of the absorbents (e.g., -OH), deposited layers (e.g., carbon), oxides (i.e., Si-OH) and sub-oxides (i.e., Si-O_2, Si-O_4) on the surface. Although a high surface hardness is observed at a lower activation time (i.e., high bondability region), the role of hardness on bondability needs further investigation.

Acknowledgments

This research is supported by discovery grants from the Natural Science and Engineering Research Council (NSERC) of Canada, an infrastructure grant from the Canada Foundation for Innovation (CFI), an Ontario Research Fund for Research Excellence (ORF-RE) Funding Grant and the Canada Research Chair program. The authors gratefully acknowledge Fangfang Zhang for her help with Hybrid Plasma Bonder. Also, the authors acknowledge to Professor M J Kim, University of Texas at Dallas for his comments on preparation of the results.

References

[1] International Technology Roadmap for Semiconductors, 2012 Update Overview www.itrs.net/links/2012ITRS/2012Chapters/2012overview.pdf

[2] Kräuter G, Schumacher A and Gösele U 1998 Low temperature silicon direct bonding for application in micromechanics: bonding energies for different combinations of oxides *Sensors Actuators* A **70** 271–5

[3] Takagi H, Maeda R, Chung T R and Suga T 1998 Low-temperature direct bonding of silicon and silicon dioxide by the surface activation method *Sensors Actuators* A **70** 164–70

[4] Wei J, Nai S M L, Wong C K and Lee L C 2004 Glass-to-glass anodic bonding process and electrostatic force *Thin Solid Films* **462–3** 487–91

[5] Deen M J and Basu P K 2012 Silicon photodetectors *Silicon Photonics: Fundamentals and Devices* (Chichester: Wiley) DOI:10.1002/9781119945161.ch8

[6] Li Z, Deen M J, Fang Q and Selvaganapathy P R 2012 Design of a flat field concave-grating-based micro-Raman spectrometer for environmental applications *Appl. Opt.* **51** 6855–63

[7] Shinwari M W, Deen M J and Landheer D 2007 Study of the electrolyte-insulator-semiconductor field-effect transistor (EISFET) with applications in biosensor design *Microelectron. Reliab.* **47** 2025–57

[8] Howlader M M R, Zhang F and Deen M J 2013 Formation of gallium arsenide nanostructures in Pyrex glass *Nanotechnology* **24** 315301

[9] Shinwari M W, Zhitomirsky D, Deen I A, Selvaganapathy P R, Deen M J and Landheer D 2010 Microfabricated reference electrodes and their biosensing applications *Sensors* **10** 1679–715

[10] Safari S, Selvaganapathy P R and Deen M J 2013 Microfluidic reference electrode with free-diffusion liquid junction *J. Electrochem. Soc.* **160** B177–83

[11] Campos F S, Faramarzpour N, Marinov O, Deen M J and Swart J W 2013 Photodetection with gate-controlled lateral BJTs from standard CMOS technology *IEEE Sens. J.* **13** 1554–63

[12] Howlader M M R, Selvaganapathy P R, Deen M J and Suga T 2011 Nanobonding technology toward electronic, fluidic, and photonic systems integration *IEEE J. Sel. Top. Quantum Electron.* **17** 689–703

[13] Suni T, Henttinen K, Suni I and Mäkinen J 2002 Effects of plasma activation on hydrophilic bonding of Si and SiO_2 *J. Electrochem. Soc.* **149** G348

[14] Byun K Y, Ferain I and Colinge C 2010 Effect of free radical activation for low temperature Si to Si wafer bonding *J. Electrochem. Soc.* **157** H109

[15] Reiche M, Gösele U and Wiegand M 2000 Modification of Si (1 0 0)-surfaces by SF6 plasma etching – application to wafer direct bonding *Cryst. Res. Technol.* **35** 807–21

[16] Tang Z, Peng P, Shi T, Liao G, Nie L and Liu S 2009 Effect of nanoscale surface topography on low temperature direct wafer bonding process with UV activation *Sensors Actuators* A **151** 81–86

[17] Dhayal M, Jeong H G and Choi J S 2005 Use of plasma polymerisation process for fabrication of bio-MEMS for micro-fluidic devices *Appl. Surf. Sci.* **252** 1710–5

[18] Howlader M M R, Kibria M G, Zhang F and Kim M J 2010 Hybrid plasma bonding for void-free strong bonded interface of silicon/glass at 200 °C *Talanta* **82** 508–15

[19] Howlader M M R, Kagami G, Lee S H, Wang J G, Kim M J and Yamauchi A 2010 Sequential plasma-activated bonding mechanism of silicon/silicon wafers *J. Microelectromech. Syst.* **19** 840–8

[20] Li J, Cui Z and Baker M 2004 A study of the surface chemistry, morphology and wear of silicon based MEMS *Surf. Interface Anal.* **36** 1254–8

[21] Ardito R, Corigliano A and Frangi A 2009 On the analysis of spontaneous adhesion in MEMS *EuroSimE '09 : 10th Int. Conf. on Thermal, Mechanical and Multi-Physics Simulation and Experiments in Microelectronics and Microsystems* pp 1–7

[22] Tong Q-Y 1997 The role of surface chemistry in bonding of standard silicon wafers *J. Electrochem. Soc.* **144** 384

[23] Ueda M, Lepienski C, Rangel E, Cruz N and Dias F 2002 Nanohardness and contact angle of Si wafers implanted with N and C and Al alloy with N by plasma ion implantation *Surf. Coat. Technol.* **156** 190–4

[24] Trevino K J, Shearer J C, Tompkins B D and Fisher E R 2011 Comparing isoelectric point and surface composition of plasma modified native and deposited SiO_2 films using contact angle titrations and x-ray photoelectron spectroscopy *Plasma Process. Polym.* **8** 951–64

[25] Christensen T B, Pedersen C M, Gröndahl K G, Jensen T G, Sekulovic A, Bang D D and Wolff A 2007 PCR biocompatibility of lab-on-a-chip and MEMS materials *J. Micromech. Microeng.* **17** 1527–32

[26] Feng Y, Zhou Z, Ye X and Xiong J 2003 Passive valves based on hydrophobic microfluidics *Sensors Actuators* A **108** 138–43

[27] Gui C, Elwenspoek M, Tas N and Gardeniers J G E 1999 The effect of surface roughness on direct wafer bonding *J. Appl. Phys.* **85** 7448

[28] Tseng A A 2006 Effects of surface roughness and oxide layer on wafer bonding strength using transmission laser bonding technique *ITHERM '06 : Therm. Thermomechanical Proc. 10th Intersoc. Conf. Phenom. Electron. Syst* pp 1349–57

[29] Kundu P, Ghosh A, Das S and Bhattacharyya T K 2012 Compatibility study of thin passivation layers with hydrazine for silicon-based MEMS microthruster *J. Phys. D. Appl. Phys.* **45** 095302

[30] Allameh S, Gally B, Brown S and Soboyejo W 2001 Surface topology and fatigue in Si MEMS structures *Mechanical Properties of Structural Films* ed C L Muhlstein and S Brown (West Conshohocken, PA: ASTM International) pp 3–16

[31] Tapily K, Baumgart H, Gu D, Elmustafa A, Krause M and Petzold M 2008 Effect of wafer bonding and layer splitting on nanomechanical properties of standard and strained SOI films *ECS Trans.* **16** 337–45

[32] Su W S, Huang H Y and Fang W 2007 Tuning the mechanical properties of SiO_2 thin film using plasma treatments for MEMS applications *Digest of papers Microprocesses and Nanotechnology* vol 8483 pp 498–9

[33] Zhang F, Kibria M G, Cormier K and Howlader M 2010 Surface and interface characterization of sequentially plasma activated silicon, silicon dioxide and germanium wafers for low temperature bonding applications *ECS Transactions* vol 33 pp 329–38

[34] Howlader M M R, Suehara S and Suga T 2006 Room temperature wafer level glass/glass bonding *Sensors Actuators* A **127** 31–36

[35] Luo S and Wong C P 2005 Influence of temperature and humidity on adhesion of underfills for flip chip packaging *IEEE Trans. Compon. Packag. Technol.* **28** 88–94

[36] Kibria M G 2010 Sequentially plasma activated bonding for wafer scale nano-integration *MASc Thesis* McMaster University http://digitalcommons.mcmaster.ca/opendissertations/4203

[37] Darrin A G and Osiander R 2011 *MEMS Materials and Processes Handbook* vol 1 (Boston, MA: Springer) pp 879–923

[38] Dimitrov A, Kralchevsky P, Nikolov A, Noshi H and Matsumoto M 1991 Contact angle measurements with sessile drops and bubbles *J. Colloid Interface Sci.* **145** 279–82

[39] Shimadzu SHIMADZU Dynamic Ultra-micro Hardness Tester www.ssi.shimadzu.com/products/literature/Testing/DUH-211_211S.pdf

[40] Fischer-Cripps A C 2011 *Nanoindentation* vol 1 (New York, NY: Springer) pp 21–38

[41] Howlader M M R, Suga T, Itoh H, Lee T H and Kim M J 2009 Role of heating on plasma-activated silicon wafers bonding *J. Electrochem. Soc.* **156** H846

[42] Choi S, Choi W, Lee Y and Ju B 2001 Effect of oxygen plasma treatment on anodic bonding *J. Korean Phys. Soc.* **38** 207–9

[43] Ma X, Chen C, Liu W, Liu X, Du X, Song Z and Lin C 2009 Study of the Ge wafer surface hydrophilicity after low-temperature plasma activation *J. Electrochem. Soc.* **156** H307

[44] Kim D-I, Kim K-H and Ahn H-S 2010 Tribological properties of adsorbed water layer on silicon surfaces *Int. J. Precis. Eng. Manuf.* **11** 741–6

[45] Moriceau H, Rieutord F, Morales C and Charvet A M 2005 Surface plasma treatments enabling low temperature direct bonding *Microsyst. Technol.* **12** 378–82

[46] Miki N and Spearing S M 2003 Effect of nanoscale surface roughness on the bonding energy of direct-bonded silicon wafers *J. Appl. Phys.* **94** 6800

[47] Howlader M M R, Zhang F and Kibria M G 2010 Void nucleation at a sequentially plasma-activated silicon/silicon bonded interface *J. Micromech. Microeng.* **20** 065012

[48] Pussadee N 2010 Poly(dimethylsiloxane) Based Micro- and Nanofluidic Device Fabrication for Electrophoresis Applications *PhD Thesis* Ohio State University https://etd.ohiolink.edu/ap:10:0::NO:10:P10_ACCESSION_NUM:osu1268179904

[49] Tayebi N and Polycarpou A A 2004 Modeling the effect of skewness and kurtosis on the static friction coefficient of rough surfaces *Tribol. Int.* **37** 491–505

[50] Alsem D H, Xiang H, Ritchie R O and Komvopoulos K 2012 Sidewall adhesion and sliding contact behavior of polycrystalline silicon microdevices operated in high vacuum *J. Microelectromech. Syst.* **21** 359–69

[51] Kibria M G, Zhang F, Lee T H, Kim M J and Howlader M M R 2010 Comprehensive investigation of sequential plasma activated Si/Si bonded interfaces for nano-integration on the wafer scale *Nanotechnology* **21** 134011

[52] Alam A U, Howlader M M R and Deen M J 2013 Oxygen plasma and humidity dependent surface analysis of silicon, silicon dioxide and glass for direct wafer bonding *ECS J. Solid State Sci. Technol.* **2** P515–23

[53] Pasquariello D, Hedlund C and Hjort K 2000 Oxidation and induced damage in oxygen plasma *in situ* wafer bonding *J. Electrochem. Soc.* **147** 2699

[54] Esser R H, Hobart K D and Kub F J 2003 Improved low-temperature Si-Si hydrophilic wafer bonding *J. Electrochem. Soc.* **150** G228

[55] Plach T, Hingerl K, Tollabimazraehno S, Hesser G, Dragoi V and Wimplinger M 2013 Mechanisms for room temperature direct wafer bonding *J. Appl. Phys.* **113** 094905

[56] Eaton W and Smith J 1997 Micromachined pressure sensors: review and recent developments *Smart Mater. Struct.* **6** 530

[57] Fang H-B, Liu J-Q, Xu Z-Y, Dong L, Wang L, Chen D, Cai B-C and Liu Y 2006 Fabrication and performance of MEMS-based piezoelectric power generator for vibration energy harvesting *Microelectron. J.* **37** 1280–4

[58] Dragoi V, Mittendorfer G, Thanner C and Lindner P 2007 Wafer-level plasma activated bonding: new technology for MEMS fabrication *Microsyst. Technol.* **14** 509–15

[59] Li X, Bhushan B, Takashima K, Baek C-W and Kim Y-K 2003 Mechanical characterization of micro/nanoscale structures for MEMS/NEMS applications using nanoindentation techniques *Ultramicroscopy* **97** 481–94

[60] Chen S H, Liu L and Wang T C 2007 Small scale, grain size and substrate effects in nano-indentation experiment of film–substrate systems *Int. J. Solids Struct.* **44** 4492–504

[61] Ligenza J R 1962 Oxidation of silicon by high-pressure steam *J. Electrochem. Soc.* **109** 73

[62] Howlader M M R and Doyle T E 2012 Low temperature nanointegration for emerging biomedical applications *Microelectron. Reliab.* **52** 361–74

[63] Nix W D 1997 Elastic and plastic properties of thin films on substrates: nanoindentation techniques *Mater. Sci. Eng.* A **234–236** 37–44

[64] Holmes D P, Tavakol B, Froehlicher G and Stone H a 2013 Control and manipulation of microfluidic flow via elastic deformations *Soft Matter* **9** 7049